Temperature and Size-Dependence of Membrane Molecular Dynamics in Unilamellar Vesicles by Fast Field-Cycling NMR Relaxometry

ARTICLE *in* THE JOURNAL OF PHYSICAL CHEMISTRY B · MARCH 2011

Impact Factor: 3.3 · DOI: 10.1021/jp2009034 · Source: PubMed

4 AUTHORS, INCLUDING:

Josefina Perlo
RWTH Aachen University
15 PUBLICATIONS **174** CITATIONS
SEE PROFILE

Dermot Brougham
Dublin City University
63 PUBLICATIONS **1,026** CITATIONS
SEE PROFILE

THE JOURNAL OF PHYSICAL CHEMISTRY B

ARTICLE

pubs.acs.org/JPCB

Temperature and Size-Dependence of Membrane Molecular Dynamics in Unilamellar Vesicles by Fast Field-Cycling NMR Relaxometry

Josefina Perlo,[†,∥] Carla J. Meledandri,[‡,§,∥] Esteban Anoardo,[*,†] and Dermot F. Brougham[*,‡]

[†]Laboratorio de Relaxometría y Técnicas Especiales, Grupo de Resonancia Magnética Nuclear, Facultad de Matemática, Astronomía y Física, Universidad Nacional de Córdoba and IFEG (CONICET), Córdoba, Argentina

[‡]National Institute for Cellular Biotechnology, School of Chemical Sciences, Dublin City University, Dublin 9, Ireland

[§]Department of Chemistry, University of Otago, Dunedin, New Zealand

Supporting Information

ABSTRACT: New methods to study dynamics in lipid bilayers are of interest particularly where they may bridge the gap between conventional experimental techniques and molecular dynamics simulations. Fast field cycling nuclear magnetic resonance relaxometry can provide valuable information as it is sensitive to dynamic processes that occur over a broad time scale. By analysis of data recorded for large unilamellar liposomes composed of 1,2-dimyristoyl-*sn*-glycero-3-posphocholine (DMPC) or 1,2-dioleoyl-*sn*-glycero-3-posphocholine (DOPC) at different temperatures and sizes, we validate an evidence-based approach to studying dynamics by relaxometry. Specifically, the number and form of the spectral density contributions from a range of dynamic processes are determined. This success of the approach strongly suggests its general applicability for the study of dynamics in membranes of more complex composition and for parameterizing molecular dynamics simulations.

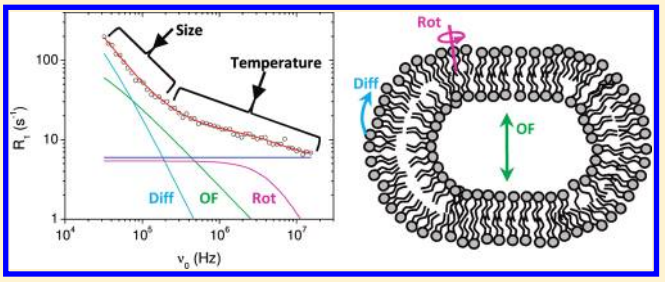

INTRODUCTION

Biomembranes are complex structures consisting primarily of a variety of lipids and proteins. The molecules can arrange in a number of different conformations giving rise to complex phase behavior and in some cases the emergence of domain structure;[1] both of these physical attributes are now known[2] to be critical for membrane function. Furthermore, membranes are dynamic assemblies[3] with significant molecular (microscopic) and cooperative (mesoscopic) mobility. Molecular and cooperative dynamics are known to influence the viscoelastic and hydrodynamic properties. For these reasons the study of membrane structure and dynamics has retained tremendous relevance across biology, chemistry, and biophysics.

The microscopic and mesoscopic fluctuations in biomembranes occur over a broad time scale, covering almost 20 decades from 10^{-15} s for molecular vibrations, to $>10^5$ s for the trans-bilayer flip-flop process of lipid molecules.[4] While many physicochemical techniques have been used for the characterization of membrane dynamics, most of these are only capable of monitoring a single aspect of the dynamics on a very limited time scale. Examples include Raman and infrared spectroscopy, electron paramagnetic resonance and fluorescence recovery after photobleaching (FRAP).[5] So while these techniques can reveal information about the microscopic molecular dynamics in membrane systems, they may obscure cooperative mesoscale dynamic features that only become apparent over longer time scales. Furthermore, with increasing computational power, molecular dynamics simulations running into the microsecond range are becoming possible. However, today this possibility is limited to a restricted quantity of molecules, thus preventing the observation of collective dynamical features and membrane curvature effects. In time it will be possible to compute into the time range where mesoscale dynamics evolve while simulating the collective behavior. Experimentally determined dynamic data acquired over a wide time scale will therefore be required for validation of molecular dynamics. Clearly experimental techniques which cover a broad range of time scales, while being sensitive to the microscopic and the mesoscopic behavior, are preferable.

Fast field-cycling nuclear magnetic resonance relaxometry (FFC-NMR), in which the spin−lattice relaxation rate (R_1) is recorded as a function of magnetic field strength ($\mathbf{B}_0$), and hence ^{1}H Larmor frequency ($\nu_L = \gamma^H\mathbf{B}_0/2\pi$), has emerged as an optimal technique with these advantages. It has been successfully applied to study dynamics in an extensive range of systems.[6] The dynamic information is obtained from the macroscopic evolution

Received: January 27, 2011
Revised: February 24, 2011
Published: March 15, 2011

of the net magnetization of the whole sample. This is strictly related to the evolution of the nuclear spins and the interactions between them, which are modulated by the molecular dynamics. So given a realistic model for the dynamic processes, NMR relaxation theory[7] allows interpretation of the measured relaxation times. There have been a few reports[8−10] of the use of FFC-NMR to study the molecular dynamics in biomembranes or membrane models. Despite experimental limitations and the absence of appropriate dynamic models, at the time, these studies demonstrated that the ^{1}H spin−lattice relaxation is of dipolar nature and is driven by the individual and collective motions of the membranes.

In recent work, we demonstrated the potential of FFC-NMR for investigating lipid dynamics and rheological properties of model membranes.[11] By applying an evidence-based approach it was possible to interpret the ^{1}H spin−lattice relaxation rate dispersions (R_1 as a function of ν_L) of large unilamellar vesicles (LUVs), of ∼50 nm radius formed from two lipid types; either 1,2-dioleoyl-*sn*-glycero-3-phosphocholine (DOPC), or 1,2-dimyristoyl-*sn*-glycero-3-phosphocholine (DMPC). The study demonstrated conclusively that in the liquid crystalline (L_α) phase relaxation dispersions, recorded over three decades of frequency, arise from modulation of the ^{1}H−^{1}H dipolar interactions due to well-known dynamical processes. Quantitative agreement between experimental and simulated dispersions was obtained by using literature values for the relevant parameters, from other experimental techniques. Thus, we demonstrated that a model where molecular and collective motions are defined, and the critical physicochemical parameters are taken from the literature, can reproduce the NMR relaxometry profiles of liposomes composed of single type of lipid.

It is known that both the curvature of the membrane and the temperature may affect the viscoelastic properties of the membrane. Upon heating, lipid membranes undergo a highly cooperative melting transition from a close packed, solid-like rippled gel ($P_{\beta'}$) phase to a disordered fluid liquid crystalline (L_α) phase, characterized by a loss of conformational order.[12] Above the transition temperature, Tm, there is a significant increase in the mobility, and therefore alkyl chain disorder, and there is significant internal rotation about the C−C bonds. The temperature dependence of some of the dynamic processes in the L_α phase has been studied using different experimental techniques. Frap[13] and pulsed field gradient NMR[14,15] were used to study lateral diffusion in macroscopically oriented lipid bilayers at temperatures $T \gg T_m$, and at $-3 < T < T_m + 3$ °C. The diffusion coefficient in both DMPC and DOPC tends to increase with temperature within both of these regimes. The bending elasticity is also temperature dependent.[16] In this paper we extend the NMR approach to interpret size and temperature dependencies of the relaxation dispersions, recorded in the L_α phase, of large unilamellar vesicles (LUVs) of different composition. The success of this study further establishes the methodology, and makes possible the study of viscoelastic properties in more complex LUV formulations. That will be the subject of forthcoming work.

THEORETICAL BACKGROUND

The spin−lattice relaxation time for an orientationally averaged sample can be expressed[7] as

$$\frac{1}{T_1} = K[J_1(\omega) + 4J_2(2\omega)] \quad (1)$$

where $K = (9/8r^6)\gamma^4\hbar^2(\mu_0/4\pi)^2$, r is the mean interproton distance, γ the proton gyromagnetic ratio, $\hbar$ the Plank's constant divided by 2π, and μ_0 the vacuum magnetic permeability. $\omega = 2\pi\nu = 2\pi(\nu_0 + \nu_L)$, where ν_0 is the magnetic field in ^{1}H Larmor frequency units and ν_L is the offset field due to the average local field component along the quantization axis. The normal component correction is less relevant as we only consider data for magnetic fields well in excess of the local field magnitude $\mathbf{B}_L$.

We will analyze the relaxation rate dispersions in terms of the dynamical processes (and the corresponding models) already considered in our previous work.[11] These relaxation mechanisms are accepted as being present in lipid membranes.

1. Order Fluctuations. In the limit of slight deformations, quasi-spherical fluctuations in unilamellar vesicles are well established as the main order fluctuation mechanism through transverse nuclear spin relaxation studies.[17,18] The corresponding spectral density can be expressed[19] as

$$J_{OF}(\omega) = \frac{k_B T}{2\pi\kappa}\sum_{l=2}^{l_{max}} \frac{l(l+1)(2l+1)}{(l^2+l-2)(l^2+l+\sigma)}\frac{\tau_l}{(1+\omega^2\tau_l^2)} \quad (2)$$

Here κ is the bending elastic modulus, k_B is the Boltzmann constant, T is the temperature, σ is the effective lateral tension, and τ_l is given by

$$\tau_l = \frac{\eta R_0^3}{\kappa}\frac{(2l+1)(2l^2+2l-1)}{l(l+1)(l+2)(l-1)(l^2+l+\sigma)} \quad (3)$$

where η is the viscosity of the supporting fluid and $l_{max} \approx \pi R_0/a$, where a is the average distance between neighboring molecules and R_0 is the average radius of the spherical liposomes.

2. Diffusion on a Curved Surface (Small Liposomes). For the case of isotropic micellar solutions, the theory proposed by Halle for spin relaxation due to diffusion on curved surfaces[20] reduces to

$$J_D(\omega) = \frac{1}{5}\left[\frac{\tau_D}{1+(\omega\tau_D)^2} + 4\frac{\tau_D}{1+(\omega\tau_D)^2}\right] \quad (4)$$

where τ_D is the joint correlation time related to the rotational-diffusion correlation time, τ_{RD}, and the surface-diffusion correlation time, τ_{TD}, by

$$\frac{1}{\tau_D} = \frac{1}{\tau_{RD}} + \frac{1}{\tau_{TD}} \quad (5)$$

with

$$\tau_{RD} = \frac{4\pi\eta R_0^3}{3k_B T} \quad \tau_{TD} = \frac{R_0^2}{6D} \quad (6)$$

D is the molecular translational diffusion coefficient, which can be estimated from the classical analysis of Brownian motion within the hydrodynamic regime.[21]

3. Molecular Rotations. We assume this contribution to be of Lorentzian type

$$J_R(\omega) = \left[\frac{\tau_R}{1+(\omega\tau_R)} + 4\frac{\tau_R}{1+(2\omega\tau_R)}\right] \quad (7)$$

4. Fast Motions. Correlation times associated with fast motions range typically from 10^{-10} s to 10^{-12} s. For this reason, within the frequency range of our experiments, they contribute with a frequency independent term.

Neglecting cross correlation terms between order fluctuations and diffusion, and invoking statistical independence of the faster motions we approximate[11] the effective relaxation rate dispersion to

$$R_1 = \frac{1}{T_1} = A_{OF}J_{OF}(\omega) + A_D J_D(\omega) + A_R J_R(\omega) + A_{FM}J_{FM}(\omega) \quad (8)$$

where $J_{OF}(\omega)$ is given by eqs 2 and 3, $J_D(\omega)$ by eqs 4−6, $J_R(\omega)$ by eq 7, and A_{FM} $J_{FM}(\omega)$ is a constant. The A_j values are the corresponding amplitude prefactors, defined as $(9/8r_j^6)\gamma^4\hbar^2$-$(\mu_0/4\pi)^2$, where r_j is the effective interproton distance for the relevant dynamic process.

EXPERIMENTAL SECTION

Reagents. 1,2-Dioleoyl-*sn*-glycero-3-phosphocholine (DOPC) and 1,2-dimyristoyl-*sn*-glycero-3-phosphocholine (DMPC) were purchased as lyophilized powders (>99%) from Avanti Polar Lipids (Alabaster, AL) and stored at −20 °C. Deuterium oxide (D_2O, purity 99.9%) was obtained from Apollo Scientific Limited (U.K.). All reagents were used without further purification.

Liposome Preparation. DOPC and DMPC LUV suspensions of different vesicle sizes, ranging from 50 to 120 nm in diameter, were prepared using established techniques. Uniform mixtures were prepared by dissolving ∼70 mg DOPC, or DMPC, in 2 mL $CHCl_3$. The solvent was removed under a slow stream of N_2 over 24 h. Liposomes were prepared by hydrating the mixtures in 1.5 mL deuterium oxide (5 M proton, 0.06 M lipid) under a constant flow of Ar. The residual 0.1% HDO in the D_2O corresponds to a ^{1}H concentration of c. 0.05M. Hence the ratio of lipid to HDO ^{1}H is ∼100:1 and we can be confident that the measured ^{1}H signal arises from the lipid ^{1}H component. The suspensions were heated above the main phase transition, T_m, to ∼22 °C for DOPC and ∼35 °C for DMPC for 24 h, followed by three heating/cooling/shaking cycles to ensure a homogeneous preparation. Following hydration, the vesicle solutions were exposed to 6 freeze−thaw cycles using liquid N_2 and warm water (40 °C), then passed through an Avanti Polar Lipids mini extruder (Alabaster, AL) containing polycarbonate membranes with a pore size of 0.2 or 0.1 μm (Whatman Nuclepore; Clifton, NJ). The extrusion process was carried out above T_m in an AtmosBag glovebag (Aldrich Chemical Co.; Milwaukee, WI).

Dynamic Light Scattering. The average sizes of the unilamellar liposome suspensions were determined using a High Performance Particle Sizer HPPS (Malvern Instruments, Malvern, U.K.) using a detection angle of 173° and a 3 mW He−Ne laser operating at a wavelength of 633 nm. The mean hydrodynamic diameter is based upon the intensity of scattered light.

Relaxation Rate Dispersion Experiments. ^{1}H relaxation rate dispersions (also termed NMRD dispersions) were measured using the FFC-NMR technique[6] with a Spinmaster FFC-2000 Fast Field Cycling NMR Relaxometer (Stelar, Mede, Italy) for liposome samples of 1 mL volume. In all cases a polarization magnetic field of 0.329 T (equivalent to 14 MHz for ^{1}H) was used, which was switched on for a period of 0.5 s to generate sample magnetization. The value of the acquisition field was 0.217 T (9.25 MHz). A field slew rate of 0.47 T.ms^{-1} (20 MHz. ms^{-1}) was used in all cases, with a switching time of 1.5 ms to allow the magnetic field to settle. A digitization rate of 1 MHz was used for acquisition, while the dead time of the spectrometer was about 20 μs. The FID was sampled with 512 points in the time range 25−540 μs, after the front edge of the 90° pulse, which was of 7.5 μs duration.

The relaxation rates, R_1, were determined from the magnetization recovery curves by least-squares fitting. The R_1 values were not sensitive to the time window over which the FID was sampled. The spin relaxation process for all samples was found to be monoexponential, within error, at all frequencies. Sample temperature was controlled to within about 0.5 K using the Spinmaster Variable Temperature Controller. Temperatures were calibrated externally using a Cu−Al thermocouple in a 10 mm NMR tube. The time for each experiment is limited by the stability of the suspensions, after several days changes were observed in both T_1 and the hydrodynamic size. For the data presented there were typically 64 repeat scans at each frequency and the total measurement time was 24 h, during which time the suspensions were unchanged. Relaxation rates dispersions were measured within the frequency range from 30 kHz to 15.2 MHz in the liquid crystalline phase.

Simulation of the Relaxation Dispersions. For this task we adopted the systematic approach[11] developed previously: (i) Fix the relevant physical parameters within their most probable intervals, using the literature values. (ii) Adjust the frequency-independent contribution to the optimal parameter set within their most probable intervals. (iii) Make fine adjustments to the amplitudes (prefactors) of each spectral density contribution, if required, see eq 8. This was done manually by observing the effect of minor adjustments on the agreement between the simulation and experimental data.

Measurement of the Local Field. The average value of the local field, deduced from the fixed-lock relaxation technique in the rotating frame, was used to determine the minimum Larmor frequency of the relaxation rate dispersions, as described in our previous work.[11] This indicated a value of 11−12 kHz for DOPC and DMPC LUVs of radius 50 and 54 mm, respectively. No systematic measurements were performed as a function of liposome diameter and temperature. However, it was verified that the average local field tends to decrease at higher temperatures and diameters. So $\mathbf{B}_{loc}$ could reliably be fixed at 11 kHz. In the simulated dispersions, it was verified that variations in the value of $\mathbf{B}_{loc}$ used, of up to 7 kHz, did not affect the main physical parameters (elastic constant, diffusion constant, and correlation times); only the relative amplitudes of the contributions required minor adjustment.

RESULTS

1. Size Dependence of LUV ^{1}H Relaxation Rate Dispersions. In Figure 1 relaxation dispersions recorded at 298 K for DOPC LUVs of different average hydrodynamic sizes are presented. It is clear that there is almost no size dependence of R_1 for $\nu_0 > 200$ kHz, but there is an increase in R_1 for smaller LUVs, at $\nu_0 < 100$ kHz. This effect is more marked for liposomes of average hydrodynamic radius $R_0 = 50$ nm. These observations indicate that the motions which determine the ^{1}H relaxation at high frequency are unaffected by changes in membrane curvature, over the size range studied, but that this is not the case at low frequency. Very similar behavior was observed in the dispersions recorded at 310 K for DMPC LUVs over the same size range, see the Supporting Information. These temperatures are significantly above the phase transition temperatures; $T_m \sim 297$ and ∼255 K for DMPC and DOPC, respectively. We can conclude that for

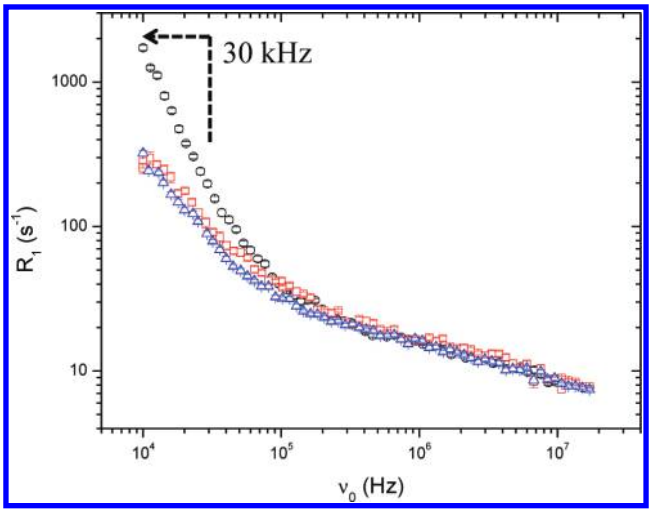

Figure 1. Experimental relaxation dispersions recorded at 298 K for DOPC LUV suspensions of average R_0 = 50 (○), 76 (□), and 120 (Δ) nm.

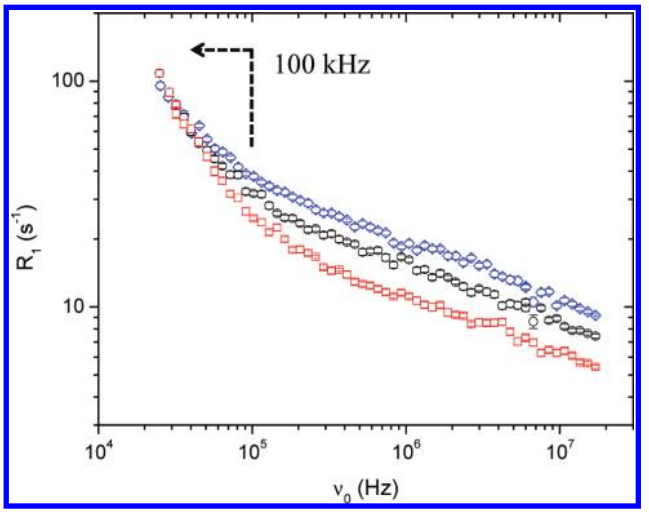

Figure 2. Experimental relaxation dispersions (ν_0 > 30 kHz) for a DOPC LUV suspension of average R_0 = 120 nm, recorded at 291 (◊), 298 (○), and 310 (□) K.

LUVs, in the L_α phase with R_0 > 100 nm, the relaxation dispersions are weakly size dependent.

Previous measurements suggest that the onset of local fields prevents measurement of the true R_1 for frequencies below 11 kHz for both DOPC and DMPC LUVs.[11] However, in the current study there were minor anomalies in a small number of the dispersions between 11 and 30 kHz. So we have taken the conservative approach of limiting the frequency range considered to ν_0 > 30 kHz. This cutoff frequency is also indicated in Figure 1. The relaxation data presented in the rest of this paper will be limited to the range 30 kHz < ν_0 < 17 MHz.

2. Temperature Dependence of ^{1}H LUV Relaxation Rate Dispersions. Relaxation dispersions recorded at 291, 298, and 310 K for a DOPC LUV suspension of R_0 = 120 nm are shown in Figure 2. It should be noted that this size is within the range where the dispersions are very weakly size dependent, Figure 1. A significant decrease in R_1 with increasing temperature is observed for ν_0 > 100 kHz. This confirms that for DOPC LUVs the

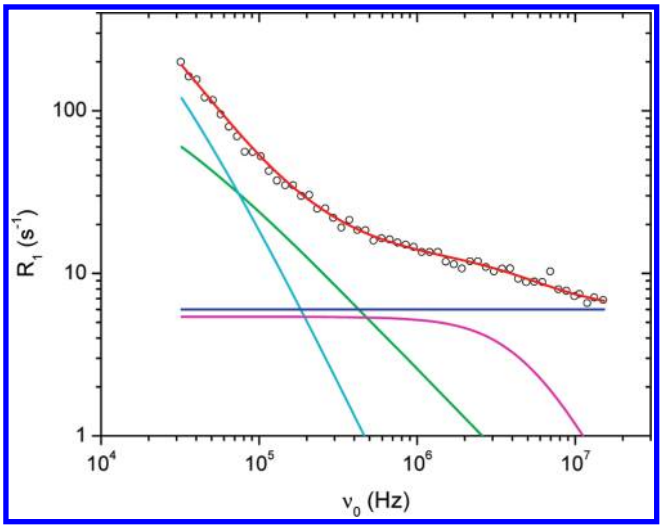

Figure 3. Experimental relaxation dispersion for a DMPC LUV sample, average R_0 = 98 nm, recorded at 310 K (○). The simulated dispersion curve is shown in red. Contributions from each type of motion are included: order fluctuations (green), diffusion (cyan), rotation (magenta), and fast motions (blue). The relevant parameters are given in Table 1.

Table 1. Parameters Corresponding to Simulations of Relaxation Dispersions Recorded at 310 K for DMPC LUVs of Different Sizes[a]

parameter		
R_0 [nm]	54	98
η D_2O [kg/s.m]	0.82×10^{-3}	0.82×10^{-3}
σ	0	0
a [nm]	1	1
κ [J]	$(3.1 \pm 0.6) \times 10^{-20}$	$(3.1 \pm 0.6) \times 10^{-20}$
A_{OF} [s^{-2}]	$(8.0 \pm 1.8) \times 10^{8}$	$(7 \pm 3) \times 10^{8}$
A_D [s^{-2}]	$(2.0 \pm 0.6) \times 10^{9}$	$(0.9 \pm 0.3) \times 10^{9}$
τ_D [s]	$(4.1 \pm 0.7) \times 10^{-5}$	$(4.0 \pm 1.1) \times 10^{-5}$
D [$m^2 s^{-1}$]	$(0.8 \pm 0.2) \times 10^{-11}$	$(3.7 \pm 1.4) \times 10^{-11}$
A_R [s^{-2}]	$(0.6 \pm 0.1) \times 10^{8}$	$(0.6 \pm 0.2) \times 10^{8}$
τ_R [s]	$(1.8 \pm 1.7) \times 10^{-8}$	$(1.8 \pm 0.7) \times 10^{-8}$
$A_{FM}J_{FM}$ [s^{-1}]	(5.5 ± 1.3)	(6 ± 1)

[a] See Figure 3.

motions which dominate at high frequency are in the motional averaging regime, $\tau_c^{-1} \gg R_1$. Over the range 100 to 30 kHz the temperature dependence gradually weakens until there is no measurable difference in R_1. As this gradual change begins at a frequency far above the local field value, the convergence can be ascribed to similarity in the spin−lattice relaxation conditions.

DISCUSSION

1. Simulating the Experimental Relaxation Rate Dispersions. A typical simulation using the approach described above, for R_0 = 98 nm DMPC LUVs recorded at 310 K, is shown in Figure 3. The spectral density contributions are also included. It is apparent that the simulation is in very close agreement with the experimental data. The parameters used in this simulation, and for DMPC LUVs of R_0 = 54 nm, are given in Table 1. In our previous work,[11] we showed that similar consistency can be

dx.doi.org/10.1021/jp2009034 |J. Phys. Chem. B 2011, 115, 3444–3451

achieved for data recorded for R_0 = 54 nm DMPC and 50 nm DOPC LUVs, at 310 and 298 K, respectively.

In this paper we show that, using our approach, it is possible to produce simulations that are in excellent agreement with experimental dispersions of liposomes of different composition (pure DMPC and pure DOPC), size (DMPC and DOPC), and temperature (DOPC). We hope in time to further broaden the range of compositions, temperatures, and liposome sizes to which the approach can be applied. The work we present here is a step toward demonstrating generality of the approach. DOPC was selected for the temperature study as there is a wider temperature range available within the L_α phase, significantly above T_m, and between room and physiological temperature. This is also the relevant range for liposomal drug delivery. A large number of parameters were obtained from this exercise; these are summarized in Tables 1−3. Figures presenting all of the simulations, which include the individual spectral density contributions to R_1, are provided in the Supporting Information. In all cases the values of the parameters used in the simulations were found to be consistent with those obtained from independent experimental studies, and this aspect is discussed in detail below.

2. Size Dependence of Relaxation Rate Dispersions. Data recorded at 298 K for DOPC LUVs of different average hydrodynamic sizes are shown in Figure 4, along with the critical spectral density contributions. The parameters used in the simulations are given in Table 2. We have already noted that the major differences in the relaxation dispersions occur at low frequency. Examination of Tables 1 and 2 shows that for both lipids the parameters governing the fast motions, A_R, τ_R, and $A_{FM}J_{FM}$, do not change significantly (within error) across the size range studied. Note that as the contribution from fast-motions is nondispersive over the frequency range studied the individual values of A_{FM} and J_{FM} cannot be determined. Hence, we will focus on the size dependence of the contributions from order fluctuations and diffusion, Figure 4.

For DOPC LUVs of different sizes, at 295 K, we found that (i) using values for κ within the reported range resulted in good consistency of the simulation with experiment and (ii) the data did not demand significant changes in κ to maintain the agreement across the size range studied, which suggests weak size dependence. The values ranged from $4.8 - 5.4 \times 10^{-20}$ J, which is equivalent to $12-13k_BT$. Literature values for DOPC bilayers include reports of 8.5 and 7.6×10^{-20} J, at 288 and 303 K, respectively ($T \gg T_m$ for DOPC), from X-ray scattering of LUVs and oriented layers.[22] There was also a recent report[23] of micropipet pressurization of giant bilayer vesicles, which gave a value of 8.5×10^{-20} J, at 291 K. Extrapolation of data from older osmotic pressure experiments[24] on LUVs of similar size suggests κ of 3.3×10^{-20} J, at 295 K. These reports confirm that the κ values obtained from our simulations are in the correct range and that the absence of significant size dependence is physically realistic.

For the remaining parameters we found that using values taken from independent experimental studies again produced excellent consistency between the data and simulations. We find that the data requires the correlation time for diffusive motion, τ_D, to be weakly size dependent (if at all), which is as expected, since diffusion is essentially a thermally driven process. The corre-

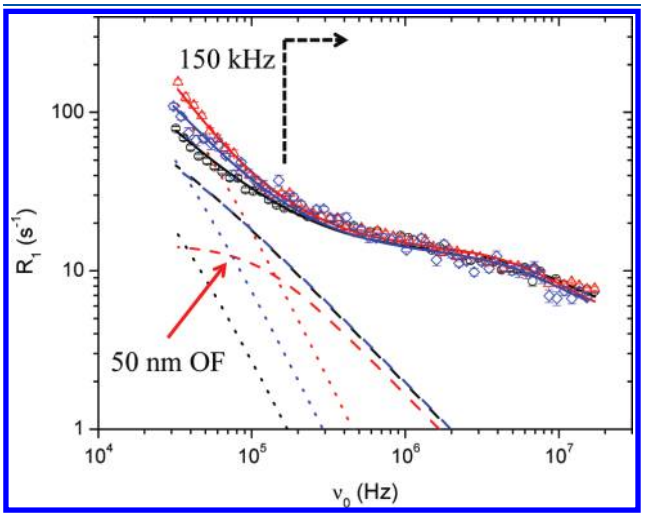

Figure 4. Experimental relaxation dispersions recorded at 298 K for DOPC LUV suspensions of average R_0 = 50 (Δ), 91 (◊), and 120 (○) nm. The simulations are shown as solid lines. The spectral density contributions for order fluctuations (dashed lines) and for diffusion (dotted lines) are included. The other spectral density contributions have been omitted for the sake of clarity. Note the plateau in the OF contribution is only apparent for R_0 = 50 nm; the OF contributions for R_0 = 91 and 120 nm are almost indistinguishable.

Table 2. Parameters Corresponding to Simulations of Relaxation Dispersions Recorded at 298 K for DOPC LUVs of Different Sizes[a]

parameter			
R_0 [nm]	50	91	120
η D_2O [kg/s.m]	1.1×10^{-3}	1.1×10^{-3}	1.1×10^{-3}
σ	0	0	0
a [nm]	1	1	1
κ [J]	$(5.4 \pm 0.9) \times 10^{-20}$	$(5.4 \pm 0.8) \times 10^{-20}$	$(4.8 \pm 0.5) \times 10^{-20}$
A_{OF} [s^{-2}]	$(0.8 \pm 0.3) \times 10^{9}$	$(1.0 \pm 0.3) \times 10^{9}$	$(0.9 \pm 0.3) \times 10^{9}$
A_D [s^{-2}]	$(1.5 \pm 0.3) \times 10^{9}$	$(0.6 \pm 0.2) \times 10^{9}$	$(0.3 \pm 0.1) \times 10^{9}$
τ_D [s]	$(7 \pm 1) \times 10^{-5}$	$(7 \pm 3) \times 10^{-5}$	$(8 \pm 4) \times 10^{-5}$
D [m^2 s^{-1}]	$(0.3 \pm 0.2) \times 10^{-11}$	$(1.8 \pm 1.5) \times 10^{-11}$	$(3 \pm 2) \times 10^{-11}$
A_R [s^{-2}]	$(1.6 \pm 0.4) \times 10^{8}$	$(1.4 \pm 0.3) \times 10^{8}$	$(1.5 \pm 0.3) \times 10^{8}$
τ_R [s]	$(1.1 \pm 0.3) \times 10^{-8}$	$(1.1 \pm 0.3) \times 10^{-8}$	$(1.0 \pm 0.2) \times 10^{-8}$
$A_{FM}J_{FM}$ [s^{-1}]	(5 ± 1)	(5 ± 1)	(5 ± 1)

[a] See Figure 4.

dx.doi.org/10.1021/jp2009034 |J. Phys. Chem. B 2011, 115, 3444–3451

sponding diffusion coefficient increases significantly with size, due to reduced curvature of the larger LUVs. The values for D of $0.3-3.0 \times 10^{-11}$ m^2 s^{-1} are physically reasonable. Lateral diffusion coefficients have been measured directly by pulsed field gradient NMR for oriented planar DOPC bilayers in this temperature range;[14] values in the range of $7-15 \times 10^{-12}$ m^2 s^{-1} were reported. The success of our approach in reproducing the data using physically realistic values for the relevant parameters suggests that physical meaning can be attributed to the changes in the spectral density contributions.

Having established physical relevance, Figure 4 demonstrates that there are two identifiable dynamic regimes. For $\nu_0 > 150$ kHz, order fluctuations clearly dominate over diffusion and, in this frequency range, the contribution of the former is weakly sensitive to changes in size. This observation is in full agreement with theoretical predictions.[19] In the lower frequency range, the situation remains the same for the larger sized LUVs, but a crossover occurs between $R_0 = 91$ and 50 nm. For $R_0 = 50$ nm the spectral density contribution from order fluctuations is reduced and a clear plateau is apparent. Again, this is in agreement with the expectations of the theoretical model. Physically, the plateau indicates a cutoff for shape fluctuations as the membranes approach the elastic limit, presumably due to increased curvature.

When our attention is turned to the contribution from diffusion, the simulations demonstrate an increase in the intensity factor A_D, which determines the strength of the contribution from diffusion, with decreasing size. This change, which is essential for reproducing the experimental behavior, is equivalent to a slight decrease in the effective interproton distance for higher curvature. This finding can be ascribed to the strong change in the diffusion regime with the curvature. For instance, the diffusion constant reduces from 3.7 to 0.8×10^{-11} m^2 s^{-1} for DMPC at 310 K (see Table 1) and by about one order of magnitude for DOPC at 298 K (see Table 2), when the radius is approximately doubled. The increasing contribution from diffusion and the emergence of a plateau in the contribution from order fluctuations (between $R_0 = 91$ and 50 nm) result in significant size dependence of R_1 for smaller LUVs, Figure 4.

The simulations are therefore qualitatively consistent with expectation and numerically consistent with independent experiment. Both of the effects described above for the diffusion and order fluctuation contributions to the dispersions are also observed in the simulations for DMPC LUVs, see Table 1 and the Supporting Information. For LUVs of R_0 greater than about 100 nm, these effects are weak and the profiles are essentially size independent.

3. Temperature Dependence of Relaxation Rate Dispersions. Relaxation dispersions recorded at 291, 298, and 310 K for DOPC LUVs of $R_0 = 120$ nm, are shown in Figure 2. In clear contrast with the observations for size dependence, the major effect of temperature is at higher frequency. Again, the consistency of the simulations with the experimental dispersions is very good, see Figure 5, and the parameters used are given in Table 3. The simulations show that the spectral density contributions, from order fluctuations and diffusion to the temperature dependence of the ^{1}H relaxation, are somewhat less important than the contribution from the "faster" processes.

To produce good consistency between the simulations and data we found it necessary to decrease the correlation times for both the diffusive and rotational motions, indeed this is as expected for thermally activated processes. Arrhenius analysis demonstrates very low activation energies, < 1 kJ mol^{-1}, in both

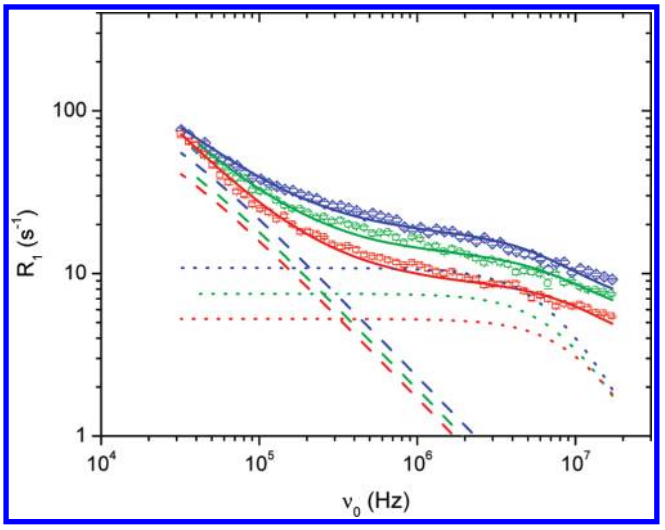

Figure 5. Experimental relaxation dispersions for a DOPC LUV suspension of average $R_0 = 120$ nm, recorded at 291 (◊), 298 (○), and 310 (□) K. The simulations are shown as solid lines. The spectral density contributions for order fluctuations (dashed lines) and for molecular rotations (dotted lines) are included. The other spectral density contributions have been omitted for the sake of clarity.

cases. The decrease in τ_D is inversely correlated with an increase in the diffusion coefficient, eq 6. The suggested increase in D, on raising the temperature from 291 to 310 K, is 41%. This compares reasonably with the 101% increase in the diffusion coefficient obtained over the same temperature range by pulsed field gradient NMR measurements for DOPC bilayers;[14] D_{PFG} values of 0.72 and 1.45×10^{-11} m^2 s^{-1} were reported at 291 and 310 K, respectively. As previously mentioned, the PFG studies were conducted on oriented planar membranes.

The other parameter from the simulations that is found to be strongly influenced by temperature is κ, the bending elastic modulus. As mentioned earlier, our approach yields values of κ (at room temperature) for DOPC, in good agreement with those obtained using a range of techniques. Our simulations suggest a 50% decrease in κ between 291 and 310 K; fitting κ to $\exp(+\varepsilon_K/k_BT)$ gives a value for ε_K of 4.9×10^{-20} J, or $11k_BT$, at 303 K. The recent X-ray scattering study, on DOPC LUVs and oriented bilayers,[22] also demonstrated that the membranes become less rigid (lower κ) with increasing temperature (from 298 to 318 K), although a weaker temperature dependence was reported, $\varepsilon_K = 2k_BT$. It should be borne in mind that X-ray scattering is a static structural approach and κ is extracted from the time averaged roughness of the bilayers using a model for the form factor. A separate electric deformation study[25] yielded $\varepsilon_K = 25k_BT$ for DOPC. Consensus seems to be emerging from different techniques for a range of lipids; as for instance neutron spin−echo experiments[26] on 200 nm DMPC LUVs suggested a significant (46%) decrease in κ with temperature ($\varepsilon_K = 7.6k_BT$) between 308 and 333 K, also in the L_α phase. However video-microscopy studies of giant (and hence negligible curvature) DMPC liposomes suggest no temperature dependence of κ from 298 to 313 K.[16]

Hence despite agreement in some cases there are difficulties with interpolating the viscoelastic properties of giant to small vesicles. As the elastic properties of liposomes at diameters of a few tens of nanometers are of particular interest for biomedical applications, the establishment of field-cycling NMR relaxometry

Table 3. Parameters Corresponding to Simulations of Relaxation Dispersions for 120 nm DOPC LUVs, Recorded at Different Temperatures[a]

parameter			
temperature [K]	291	298	310
η D_2O [kg/s.m]	1.3×10^{-3}	1.1×10^{-3}	0.82×10^{-3}
σ	0	0	0
a [nm]	1	1	1
κ [J]	$(6 \pm 1) \times 10^{-20}$	$(4.8 \pm 0.5) \times 10^{-20}$	$(3.0 \pm 0.7) \times 10^{-20}$
A_{OF} [s^{-2}]	(1.3 ± 0.1) x10^9	$(0.9 \pm 0.3) \times 10^9$	$(0.5 \pm 0.3) \times 10^9$
A_D [s^{-2}]	(0.1 ± 0.1) x10^9	$(0.2 \pm 0.1) \times 10^9$	$(0.2 \pm 0.2) \times 10^9$
τ_D [s]	$(9 \pm 8) \times 10^{-5}$	$(8 \pm 4) \times 10^{-5}$	$(6 \pm 5) \times 10^{-5}$
D [m^2s^{-1}]	$(2.7 \pm 1.3) \times 10^{-11}$	$(3.0 \pm 1.9) \times 10^{-11}$	$(3.8 \pm 1.8) \times 10^{-11}$
A_R [s^{-2}]	$(1.8 \pm 0.4) \times 10^8$	$(1.5 \pm 0.3) \times 10^8$	$(1.4 \pm 0.4) \times 10^8$
τ_R [s]	$(1.2 \pm 0.3) \times 10^{-8}$	$(1.0 \pm 0.2) \times 10^{-8}$	$(0.7 \pm 0.2) \times 10^{-8}$
$A_{FM}J_{FM}$ [s^{-1}]	(6 ± 2)	(5 ± 1)	(3 ± 1)

[a] See Figure 5.

may provide further insights, complementary to neutron and X-ray techniques, for liposome sizes not accessible with current videomicroscopy and micropipet approaches.

4. Overview of the Approach. There are two components to the simulation of the contribution from each dynamic process; the frequency dependence, or spectral density, and the prefactor. Whereas the former is determined by the relevant dynamic process, the prefactors are largely determined by the effective interproton distances, arising from the usual inverse sixth-power dependence. The prefactors obtained from the simulations presented correspond to effective interproton distances ranging from 2.6 to 4.7 Å. Effective interproton distances may differ for each contributing mechanism depending on the nature of the relaxation process and the location within the molecule of the dominant contributing ^{1}H nuclei.[27]

We have generally found that the size dependence of the prefactors is weak, as one would expect. The one exception is in the case of diffusion; A_D is found to decrease for smaller LUVs, as discussed above. Similarly, the temperature dependence of the prefactors is weak for both diffusion and molecular rotations. For the fast motions, $A_{FM}J_{FM}$ is found to decrease somewhat with temperature. In this particular case, changes in the prefactor may not be exclusively related to changes in the interproton distances, as the spectral density contribution it is a Lorentzian and for $\nu_0 <$ 20 MHz is within the nondispersive regime, i.e., on the plateau. Finally, the prefactor for order fluctuations, A_{OF}, is found to decrease with increasing temperature, above 291 K. The decrease was found to be by 35 and 65% at 298 and 310 K, respectively. Given the sixth power dependence these values correspond to increases in average internuclear separation with increasing temperature of 15 and 20%, as compared to 291 K.

Turning to the dynamic information provided by the simulations. Our previous work[11] has established that the approach can be used to simulate relaxation data for similarly sized LUVs, of different composition, using physically realistic values for the critical parameters, see Table 4. The current study demonstrates the robustness of the technique; we have successfully extended it to simulate relaxation dispersions for LUVs ofdifferent sizes, recorded over a range of temperatures. This lends credibility to the key assumptions of the approach: That the relevant processes are order fluctuations, diffusion, molecular rotations, and fast motions, only, and that the form of spectral density functions selected are indeed appropriate for hydrated lipid bilayers.

Table 4. Summary of the Most Probable Intervals for Each Physical Parameter with Indicative References

parameter	range	refs
η [kg/s.m]	$(0.8-1.3) \times 10^{-3}$	28 and 29
σ	0−25	19, 28, and 30
a [nm]	1−1.2	17, 18, 21, and 31
κ [J]	$4 \times 10^{-21}-10^{-19}$	32−34
A_D [s^{-2}][a]	$1.6 \times 10^7-0.4 \times 10^{10}$	8 and 35
D [m^2s^{-1}]	$10^{-10}-10^{-12}$	14, 15, 21, 29, and 36−39
A_{OF} [s^{-2}]	$1.6 \times 10^7-0.4 \times 10^{10}$	8 and 35
A_R [s^{-2}]	$1.6 \times 10^7-0.4 \times 10^{10}$	8 and 35
τ_R [s]	$10^{-10}-10^{-7}$	9, 40, and 41

[a] In all cases A_j values have been calculated using the r_j values obtained from the literature, see text.

Having established these principles the possibility of applying the approach to study the effects of compositional changes on curved membranes may now be investigated. In a great many cases, most obviously with the addition of secondary lipids as a minor component, there is a wealth of structural and phase information available. We are most interested in probing the dynamics at lipid compositions close to phase separation. The methodologies we have developed may lead to new insights into the dynamic processes in these critical situations. The advantage of FFC-NMR over other techniques, such as neutron scattering or PFG NMR which precisely measure a single aspect, is that it simultaneously provides physically meaningful information on dynamics over a range of time scales. The accessible frequency window (17 MHz to 30 kHz) covers time scales ranging from approximately nanoseconds to microseconds, which is far longer than is possible using even coarsely grained simulation techniques. We hope that in time our approach may contribute to the development of an integrated understanding of how different dynamic processes influence the emergent membrane properties.

CONCLUSIONS

FFC-NMR has been shown to be a tool particularly suited to the study and characterization of the molecular dynamics in

liposomes. The ^{1}H relaxation data of a wide range of LUV systems studied at different temperatures and of different sizes can now be interpreted in terms of a model incorporating known dynamic processes. The approach can be applied to liposomes of size below that accessible with current video-microscopy and micropipet techniques and within the range relevant to biomedical applications. We hope that the methods established in this work will provide insights into the interplay between dynamics and function in membrane systems of more complex composition.

■ ASSOCIATED CONTENT

Supporting Information. Remaining experimental and simulated relaxation dispersions, including contributions from each type of motion. This material is available free of charge via the Internet at http://pubs.acs.org.

■ AUTHOR INFORMATION

Corresponding Author

*E-mail: anoardo@famaf.unc.edu.ar; dermot.brougham@dcu.ie.

Author Contributions

‖C.J.M. and J.P. contributed equally to this work.

■ ACKNOWLEDGMENT

This work was partially supported by funds from Foncyt (PICT25765), CONICET (PIP6420), and Mincyt Córdoba (PID 2008 Res. 121) from Argentina. C.J.M. acknowledges the National Institute for Cellular Biotechnology and Enterprise Ireland (PC/2006/207) for financial support. D.B. acknowledges Enterprise Ireland (IF/2001/364, PC/2004/0429) and the Higher Education Authority of the Republic of Ireland for supporting the purchase of NMR equipment. J.P. acknowledges a fellowship granted by CONICET.

■ REFERENCES

(1) Gawrisch, K. The Structure of Biological Membranes. *The Dynamics of Membrane Lipids*; Yeagle, P.L., Ed.; CRC Press: New York, 2005; pp 540.
(2) Simons, K.; Ikonen, E. *Nature* **1997**, *387*, 569.
(3) Lee, G. M.; Jacobson, K. Cell Lipids. *Lateral Mobility of Lipids in Membranes*; Hoekstra, D., Ed.; Academic Press: New York, 1994; pp 638.
(4) Kornberg, R. D.; McConnell, H. M. *Biochemistry* **1971**, *10*, 1111.
(5) Membrane Spectroscopy; Grell, E., Ed.; Springer Verlag: Berlin, 1981.
(6) Kimmich, R.; Anoardo, E. *Progr. NMR Spectrosc.* **2004**, *44*, 257.
(7) Abragam, A. *Principles of Nuclear Magnetism*; Oxford U. P.: London, 1961.
(8) Kimmich, R.; Schnur, G.; Scheuermann, A. *Chem. Phys. Lipids* **1983**, *32*, 271.
(9) Rommel, E.; Noack, F.; Meier, P.; Kothe, G. *J. Phys. Chem.* **1988**, *92*, 2981.
(10) Struppe, J.; Noack, F.; Klose, G. *Z. Naturforsh.* **1997**, *52a*, 681.
(11) Meledandri, C. J.; Perlo, J.; Farrher, E.; Brougham, D. F.; Anoardo, E. *J. Phys. Chem. B* **2009**, *113*, 15532.
(12) Koynova, R.; Caffrey, M. *Biochim. Biophys. Acta* **1998**, *1376*, 91.
(13) Almeida, P. F. F.; Vaz, W. L. C.; Thompson, T. E. *Biochemistry* **1992**, *31*, 6739.
(14) Filippov, A.; Orädd, G.; Lindblom, G. *Biophys. J.* **2003**, *84*, 3079.
(15) Filippov, A.; Orädd, G.; Lindblom, G. *Biophys. J.* **2007**, *93*, 3182.
(16) Méléard, P.; Gerbeaud, C.; Pott, T.; Fernandez-Puente, L.; Bivas, I.; Mitov, M. D.; Dufourcq, J.; Bothorel, P. *Biophys. J.* **1997**, *72*, 2616.
(17) Althoff, G.; Frezzato, D.; Vilfan, M.; Stauch, O.; Schubert, O.; Vilfan, I.; Moro, G. J.; Kothe, G. *J. Phys. Chem. B* **2002**, *106*, 5506.
(18) Althoff, G.; Stauch, O.; Vilfan, M.; Frezzato, D.; Moro, G. J.; Hausser, P.; Schubert, R.; Kothe, G. *J. Phys. Chem. B* **2002**, *106*, 5517.
(19) Vilfan, M.; Althoff, G.; Vilfan, I.; Kothe, G. *Phys. Rev. E* **2001**, *64*, 022902.
(20) Halle, B. J. *Chem. Phys.* **1991**, *94*, 3150.
(21) Saffman, P. G.; Delbruch, M. *Proc. Natl. Acad. Sci.* **1975**, *72*, 3111.
(22) Pan, J.; Tristam-Nagle, S.; Kucerka, N.; Nagle, J. F. *Biophys. J.* **2008**, *94*, 117.
(23) Rawicz, W.; Olbrich, K. C.; McIntosh, T.; Needham, D.; Evans, D. *Biophys. J.* **2000**, *79*, 328.
(24) Chen, Z.; Rand, R. P. *Biophys. J.* **1997**, *73*, 267.
(25) Niggemann, G.; Kummrow, M.; Helfrich, W. *J. Phys. II France* **1995**, *5*, 413.
(26) Yi, Z.; Nagao, M.; Bossev, D. P. *J. Phys.: Condensed Matter* **2009**, *21*, 155104.
(27) Kühner, W.; Rommel, E.; Noack, F. *Z. Naturforsch.* **1987**, *42a*, 127.
(28) Henriksen, J.; Rowat, A. C.; Ipsen, J. H. *Eur. Biophys. J.* **2004**, *33*, 732.
(29) *Handbook of Chemistry and Physics* 74th ed.; Lide, D., Ed.; CRC Press: Boca Raton, FL, 1993−1994.
(30) Bloom, M.; Evans, E.; Mouritsen, O. G. *Q. Rev. Biophys.* **1991**, *24*, 293.
(31) Umegawa, Y.; Matsumori, N.; Oishiv, T.; Murata, M. *Biochem.* **2008**, *47*, 13463.
(32) Duwe, H. P.; Sackmann, E. *Physica A* **1990**, *163*, 410.
(33) Tristram-Nagle, S.; Petrache, H. I.; Nagle, J. F. *Biophys. J.* **1998**, *75*, 917.
(34) Liu, Y.; Nagle, J. F. *Phys. Rev. E* **2004**, *69*, 040901.
(35) Mishra, V. K.; Anantharamaiah, G. M.; Segrest, J. P.; Palgunachari, M. N.; Chaddha, M. J. *Biol. Chem.* **2006**, *281*, 6511.
(36) Tamm, K.; McConnell, H. M. *Biophys. J.* **1985**, *47*, 105.
(37) Przybylo, M.; Sýkora, J.; Humpoličková, J.; Benda, A.; Zan, A.; Hof, M. *Langmuir* **2006**, *22*, 9096.
(38) Kahya, N.; Scherfeld, D.; Bacia, K.; Schwille, P. *J. Struct. Biol.* **2004**, *147*, 77.
(39) Scherfeld, D.; Kahya, N.; Scwille, P. *Biophys. J.* **2003**, *85*, 3758.
(40) Lindahl, E.; Edholm, O. *J. Chem. Phys.* **2001**, *115*, 4938.
(41) Petersen, N. O.; Chan, S. I. *Biochemistry* **1977**, *16*, 2657.